A NURBS-based isogeometric formulation for geometrically nonlinear analysis of shells

Matheus Pascoal Martins de Sousa[1], Elias Saraiva Barroso[1], Evandro Parente Jr.[1], João Batista Marques de Sousa Junior[1], Joaquim Bento Cavalcante Neto[2].

[1]*Laboratório de Mecânica Computacional e Visualização (LMCV), Departamento de Engenharia Estrutural e Construção Civil*
Universidade Federal do Ceará, Campus do Pici, Bloco 728, 60440-900, Fortaleza/CE-Brazil
matheuspmsousa@alu.ufc.br, elias.barroso@ufc.br, evandro@ufc.br, joaobatistasousajr@ufc.br
[2]*Computer Graphics, Virtual Reality and Animation Group (CRAb), Departamento de Computação*
Universidade Federal do Ceará, Campus do Pici, Bloco 910, 60440-900, Fortaleza/CE-Brazil
joaquimb@dc.ufc.br

Abstract. This work presents a NURBS-based isogeometric formulation for geometrically nonlinear analysis of shells based on the Reissner-Mindlin theory and the degenerated solid approach. The geometrically nonlinear effects are incorporated using the Total Lagrangian approach allowing the analysis of shells with large displacement and rotations. Different numerical integrations schemes are used in order alleviate the locking problem. The accuracy of the proposed formulation is assessed using a well-known benchmark of nonlinear shells.

Keywords: Shells, Isogeometric Analysis, NURBS, Nonlinear Analysis, Locking.

1 Introduction

Shells are curved surface structures whose thickness is much smaller than other dimensions. Due to their high slenderness, shell structures are vulnerable to collapse caused by loss of stability. Thus, the structural analysis of shells should include the geometrically nonlinear effects due to large displacements and rotations.

The ability of Isogeometric Analysis (IGA) to exactly describe the geometry of the problem independent of the degree of discretization and to allow easy refinements has led to its increasing application in shell analysis. A Reissner-Mindlin formulation based on the degenerated solid approach was initially proposed by Uhm and Youn [1] for T-Splines, which was later extended to a nonlinear formulation for isogeometric analysis by Dornisch et al. [2], using exactly calculated director vectors for NURBS.

It is important to note that IGA does not remove the shear and membrane locking presented by fully integrated shell elements based on Reissner-Mindlin theory [3]. Thus, several alternatives have been proposed in the literature to address the locking problem, such as mixed formulation and reduced integration [4].

This work presents a NURBS-based isogeometric formulation for geometrically nonlinear analysis of shells based on the Reissner-Mindlin theory and the degenerated solid approach. The geometrically nonlinear effects are incorporated using the Total Lagrangian (TL) approach allowing the analysis of shells with large displacement and rotations. Furthermore, different numerical integration schemes are used in order to alleviate the locking problem. The accuracy of the proposed formulation and numerical integration schemes is assessed using a well-known benchmark of nonlinear shells.

The rest of the paper is organized as follows. Section 2 describes the nonlinear isogeometric formulation. Section 3 presents the numerical example used to assess the efficiency of the present formulation. Finally, Section 4 presents the concluding remarks of the study.

2 Isogeometric formulation

A NURBS surface is defined by a given control net $\mathbf{P}_a(n \times m)$, and knot vectors $\Xi = [\xi_1, \xi_2, ..., \xi_{n+p+1}]$ and $\Omega = [\eta_1, \eta_2, \ldots, \eta_{n+p+1}]$ as:

$$S(\xi, \eta) = \sum_{a=1}^{np} R_a(\xi, \eta)\, \mathbf{P}_a. \tag{1}$$

where np is the number of control points and $R_a(\xi, \eta)$ are the bivariate rational basis functions given by:

$$R_a(\xi, \eta) = \frac{N_{i,p}(\xi)\, N_{j,q}(\eta)\, w_{ij}}{\sum_{\hat{i}=1}^{n} \sum_{\hat{j}=1}^{m} N_{\hat{i},p}(\xi)\, N_{\hat{j},q}(\eta)\, w_{\hat{i}\hat{j}}} = \frac{N_{i,p}(\xi)\, N_{j,q}(\eta)\, w_{ij}}{W(\xi, \eta)}, \tag{2}$$

where $N_{i,p}(\xi)$ and $N_{j,q}(\eta)$ are univariate B-Splines basis functions, w_{ij} is the control point weight, and $W(\xi, \eta)$ is the bivariate weighting function. It is worth noting that the global basis index a is related to tensor product basis indexes (i, j) by:

$$a = m(i-1) + j, \qquad i = 1, 2, \ldots n, \qquad j = 1, 2, \ldots m \quad \text{and} \quad np = m\, n. \tag{3}$$

In the degenerated solid approach, the geometry of the shell at a generic time t is represented by a point $\mathbf{x}_s$ of the mid-surface and corresponding unit normal vector $\mathbf{v}_3$ and thickness h. Thus, a point $\mathbf{x}$ within the shell is defined by:

$$\mathbf{x}^t(\xi, \eta, \zeta) = \mathbf{x}_s^t(\xi, \eta) + \zeta\, \frac{h(\xi, \eta)}{2}\, \mathbf{v}_3^t(\xi, \eta), \tag{4}$$

where $-1 \leq \xi \leq +1$, $-1 \leq \eta \leq +1$ are the parametric coordinates tangent to the shell mid-surface and $-1 \leq \zeta \leq +1$ is the parametric coordinate along the thickness. Using the degenerated solid approach, the shell geometry is defined as:

$$\mathbf{x}^t = \sum_{a=1}^{np} R_a\, \mathbf{x}_a^t + \sum_{a=1}^{np} \zeta\, R_a\, \frac{h_a}{2}\, \mathbf{v}_{3a}^t \tag{5}$$

where $\mathbf{x}_a$ are the control points of the shell mid-surface, $\mathbf{v}_{3a}$ is a normal vector, and h_a the thickness associated with control point a.

Unlike finite element nodes, NURBS control points are usually not on the shell surface, complicating the definition of the director vectors and the consideration of rotational degrees of freedom. The definition of these vectors is critical for Reissner-Mindlin shells and several approaches have been proposed in the literature. Some techniques require each control point to be mapped to a corresponding point on the surface. The surface points closest to the control points and the anchor points represented in the parameter space are some of the proposed options [1, 4]. As the control points are not distributed equally in the parameter and physical spaces, these approaches provide less accurate results as the order of the basis function increases. On the other hand, the initial director vectors at the control points can be computed to provide exact interpolated director vectors at integration points, producing the desired convergence behavior [2]. Unfortunately, this procedure is complex and computationally costly. Furthermore, new directors must be computed if the numerical integration scheme is modified.

Thus, in this work a simpler approach is adopted, where the exact director vectors at the Greville points are considered as known values for the system of equations and the director vectors at control points are computed solving a simple linear equation system [4]. The so-called Greville points, $t_i = (t_{i_\xi}, t_{i_\zeta})$, define in the parameter space as [5]:

$$t_{i\xi} = \frac{\xi_{i+1} + \cdots + \xi_{i+p}}{p} \tag{6}$$

The director vectors defining the shell local system at $t = 0$ are computed as:

$$\mathbf{v}_3^0 = \frac{S_{,\xi}(t_{i\xi}, t_{i\eta}) \times S_{,\eta}(t_{i\xi}, t_{i\eta})}{||S_{,\xi}(t_{i\xi}, t_{i\eta}) \times S_{,\eta}(t_{i\xi}, t_{i\eta})||}, \qquad \mathbf{v}_1^0 = \frac{\mathbf{e}_2 \times \mathbf{v}_3^0}{||\mathbf{e}_2 \times \mathbf{v}_3^0||}, \qquad \mathbf{v}_2^0 = \mathbf{v}_3^0 \times \mathbf{v}_1^0 \tag{7}$$

where $\mathbf{v}_3^0$ is perpendicular and $\mathbf{v}_1^0$ and $\mathbf{v}_2^0$ are tangent to the initial shell midsurface.

In each Greville point, the local basis system has nine components denoted by $\mathbf{v}_{ij}^0$ (where i, j = 1, 2, 3), requiring the separate solution of nine assembled systems of equations on the patch in the following form:

$$\mathbf{v}_{ij}^{Gr}(t_{i\xi}, t_{i\eta}) = \sum_{a=1}^{np} R_a(t_{i\xi}, t_{i\eta})\, \mathbf{v}_{ija}^{cp} \qquad i, j = 1, 2, 3 \tag{8}$$

in which $\mathbf{v}_{ij}^{Gr}$ are known basis vectors at the Greville points, np is the number of control points and $\mathbf{v}_{ija}^{cp}$ are unknown basis vectors at the control points.

2.1 Displacements and strains

The displacements of a generic point within the shell is given by the difference between its coordinates at times 0 and t:

$$\mathbf{u} = \mathbf{x}^t - \mathbf{x}^0 \tag{9}$$

Considering Eq. (5), the displacement field is given by:

$$\mathbf{u} = \sum_{a=1}^{np} R_a\,\mathbf{u}_a + \sum_{a=1}^{np} \zeta\, R_a\,\frac{h_a}{2}\,\left(\mathbf{v}_{3a}^t - \mathbf{v}_{3a}^0\right) \tag{10}$$

where $\mathbf{u}_a$ are the mid-surface displacements of control points. The first term represent the effects of the mid-surface translations and the second term represent the effects of the rotations of the normal vector around $\mathbf{v}_1$ and $\mathbf{v}_2$. The displacements can be written in a compact form as:

$$\mathbf{u} = \sum_{a=1}^{np} \left(R_a\,\mathbf{u}_a + H_a\,\mathbf{p}_a\right) \tag{11}$$

where

$$H_a = \zeta\, R_a, \qquad \mathbf{p}_a = \frac{h_a}{2}\,\left(\mathbf{v}_{3a}^t - \mathbf{v}_{3a}^0\right) \tag{12}$$

Since large 3D rotations are not additive [6], the normal vector should be updated from t to $t+\Delta t$ as

$$\mathbf{v}_3^{t+\Delta t} = \mathbf{Q}\,\mathbf{v}_3^t \tag{13}$$

where $\mathbf{Q}$ is an orthogonal rotation matrix depending on the incremental rotations α and β about vectors $\mathbf{v}_1^t$ and $\mathbf{v}_2^t$. However, considering moderate rotation increments, it is possible to use the quadratic approximation [7]:

$$\mathbf{v}_3^{t+\Delta t} = \mathbf{v}_3^t - \alpha\,\mathbf{v}_2^t + \beta\,\mathbf{v}_1^t - \frac{1}{2}(\alpha^2+\beta^2)\,\mathbf{v}_3^t \tag{14}$$

where

$$\mathbf{v}_1^t = \frac{\mathbf{e}_2 \times \mathbf{v}_3^t}{||\mathbf{e}_2 \times \mathbf{v}_3^t||}, \qquad \mathbf{v}_2^t = \mathbf{v}_3^t \times \mathbf{v}_1^t \tag{15}$$

The Total Lagrangian (TL) approach [7], where the stresses and strains are evaluated in the initial configuration of the structure, is adopted in this work. This formulation is based on the use of Green-Lagrange strains and Piola-Kirchhoff II stresses. The Green-Lagrange strains are computed from the displacement derivatives with respect to the Cartesian coordinates:

$$\boldsymbol{\varepsilon} = \begin{Bmatrix} \varepsilon_x \\ \varepsilon_y \\ \varepsilon_z \\ \gamma_{xy} \\ \gamma_{xz} \\ \gamma_{yz} \end{Bmatrix} = \begin{Bmatrix} u_{,x} \\ v_{,y} \\ w_{,z} \\ u_{,y} + v_{,x} \\ w_{,x} + u_{,z} \\ v_{,z} + w_{,y} \end{Bmatrix} + \frac{1}{2} \begin{Bmatrix} u_{,x}^2 + v_{,x}^2 + w_{,x}^2 \\ u_{,y}^2 + v_{,y}^2 + w_{,y}^2 \\ u_{,z}^2 + v_{,z}^2 + w_{,z}^2 \\ 2(u_{,x}\,u_{,y} + v_{,x}\,v_{,y} + w_{,x}\,w_{,y}) \\ 2(u_{,x}\,u_{,z} + v_{,x}\,v_{,z} + w_{,x}\,w_{,z}) \\ 2(u_{,y}\,u_{,z} + v_{,y}\,v_{,z} + w_{,y}\,w_{,z}) \end{Bmatrix} \tag{16}$$

According to Eqs. (11), (12), and (16), the strains depend on the derivatives of the basis functions R_a and ζ function with respect to the Cartesian coordinates (x, y, z). However, these functions are defined in terms of parametric coordinates (ξ, η, ζ). In this work, the ζ coordinate is handled as an additional shape function and the required derivatives with respect to the Cartesian coordinates are computed from:

$$\begin{bmatrix} R_{a,x} \\ R_{a,y} \\ R_{a,z} \end{bmatrix} = \mathbf{J}^{-1} \begin{bmatrix} R_{a,\xi} \\ R_{a,\eta} \\ 0 \end{bmatrix} \quad \text{and} \quad \begin{bmatrix} \zeta_{,x} \\ \zeta_{,y} \\ \zeta_{,z} \end{bmatrix} = \mathbf{J}^{-1} \begin{bmatrix} 0 \\ 0 \\ 1 \end{bmatrix}, \tag{17}$$

where the Jacobian matrix ($\mathbf{J}$) is given by:

$$\mathbf{J} = \begin{bmatrix} \sum R_{a,\xi}\left(x_a + \zeta\dfrac{h_a}{2}v_{3x_a}\right) & \sum R_{a,\xi}\left(y_a + \zeta\dfrac{h_a}{2}v_{3y_a}\right) & \sum R_{a,\xi}\left(z_a + \zeta\dfrac{h_a}{2}v_{3z_a}\right) \\ \sum R_{a,\eta}\left(x_a + \zeta\dfrac{h_a}{2}v_{3x_a}\right) & \sum R_{a,\eta}\left(y_a + \zeta\dfrac{h_a}{2}v_{3y_a}\right) & \sum R_{a,\eta}\left(z_a + \zeta\dfrac{h_a}{2}v_{3z_a}\right) \\ \sum R_a\dfrac{h_a}{2}v_{3x_a} & \sum R_a\dfrac{h_a}{2}v_{3y_a} & \sum R_a\dfrac{h_a}{2}v_{3z_a} \end{bmatrix}. \tag{18}$$

Due to the use of the TL approach, all Jacobian calculations are carried out in the initial (i.e. underformed) geometry.

To simplify the mathematical derivations, it is interesting to write the Green-Lagrange strains, Eq. (16), as

$$\boldsymbol{\varepsilon} = \boldsymbol{\varepsilon}_0 + \boldsymbol{\varepsilon}_L = \mathbf{H}\,\boldsymbol{\beta} + \frac{1}{2}\mathbf{A}\,\boldsymbol{\beta} \tag{19}$$

where

$$\boldsymbol{\beta} = \begin{Bmatrix} u_{,x} \\ u_{,y} \\ u_{,z} \\ v_{,x} \\ v_{,y} \\ v_{,z} \\ w_{,x} \\ w_{,y} \\ w_{,z} \end{Bmatrix} = \sum_{a=1}^{np} \begin{Bmatrix} R_{a,x}\,u_a + H_{a,x}\,p_{x_a} \\ R_{a,y}\,u_a + H_{a,y}\,p_{x_a} \\ R_{a,z}\,u_a + H_{a,z}\,p_{x_a} \\ R_{a,x}\,v_a + H_{a,x}\,p_{y_a} \\ R_{a,y}\,v_a + H_{a,y}\,p_{y_a} \\ R_{a,z}\,v_a + H_{a,z}\,p_{y_a} \\ R_{a,x}\,w_a + H_{a,x}\,p_{z_a} \\ R_{a,y}\,w_a + H_{a,x}\,p_{z_a} \\ R_{a,z}\,w_a + H_{a,x}\,p_{z_a} \end{Bmatrix} \tag{20}$$

with

$$H_{a,x} = R_{a,x}\,\zeta + R_a\,\zeta_{,x}, \qquad H_{a,y} = R_{a,y}\,\zeta + R_a\,\zeta_{,y} \quad \text{and} \quad H_{a,z} = R_{a,z}\,\zeta + R_a\,\zeta_{,z}. \tag{21}$$

Due to the use of the degenerated solid approach, matrices $\mathbf{H}$ and $\mathbf{A}$ are the same ones of 3D continuum elements [8].

2.2 Stresses

Considering small strains and linear elastic behavior, the Piola-Kirchhoff II stresses can be computed from Green-Lagrange strains in the local system using the generalized Hooke's law [9]:

$$\boldsymbol{\sigma}' = \mathbf{C}'\,\boldsymbol{\varepsilon}'. \tag{22}$$

The local system (x', y', z'), where the material properties of the shell are defined, is defined by the director vectors $\mathbf{v}_1$, $\mathbf{v}_2$, and $\mathbf{v}_3$ where $\mathbf{v}_1$ and $\mathbf{v}_2$ are unit vectors tangent to the shell mid-surface.

The material properties need to be transformed to the global system of the problem, where the strain-displacement relations are defined and the equilibrium of the structure is established. Strains in global system ($\boldsymbol{\varepsilon}$) are related to local strains ($\boldsymbol{\varepsilon}'$) using the transformation matrix $\mathbf{T}$ [9]:

$$\boldsymbol{\varepsilon}' = \mathbf{T}\,\boldsymbol{\varepsilon}. \tag{23}$$

Moreover, the stresses and the constitutive matrix can be obtained in the global system in the same manner:

$$\boldsymbol{\sigma} = \mathbf{T}^T\,\boldsymbol{\sigma}' \quad \Rightarrow \quad \boldsymbol{\sigma} = \mathbf{C}\,\boldsymbol{\varepsilon} \quad \Rightarrow \quad \mathbf{C} = \mathbf{T}^T\,\mathbf{C}'\,\mathbf{T}. \tag{24}$$

2.3 Equilibrium equations

The static equilibrium equations of the model can be obtained using the Principle of Virtual Work:

$$\delta U = \delta W_{ext} \quad \Rightarrow \quad \int_V \delta\boldsymbol{\varepsilon}^T\,\boldsymbol{\sigma}\,dV = \int_V \delta\mathbf{u}^T\,\mathbf{b}\,dV + \int_S \delta\mathbf{u}^T\,\mathbf{q}\,dS, \tag{25}$$

where $\delta\mathbf{u}$ is the virtual displacement vector, $\delta\boldsymbol{\varepsilon}$ is the virtual strain vector, and $\mathbf{q}$ and $\mathbf{b}$ are the surface and body loads, respectively. The virtual strains are obtained by the variation of Eq. (19):

$$\delta\boldsymbol{\varepsilon} = \mathbf{H}\,\delta\boldsymbol{\beta} + \frac{1}{2}\,\delta\mathbf{A}\,\boldsymbol{\beta} + \frac{1}{2}\,\mathbf{A}\,\delta\boldsymbol{\beta} = \mathbf{H}\,\delta\boldsymbol{\beta} + \mathbf{A}\,\delta\boldsymbol{\beta} \tag{26}$$

On the other hand, the variation of Eq. (12) yields:

$$\delta\mathbf{p}_a = \frac{h_a}{2}\,\delta\mathbf{v}_{3a}^t = \mathbf{p}_a^\alpha\,\delta\alpha + \mathbf{p}_a^\beta\,\delta\beta \tag{27}$$

where

$$\mathbf{p}_a^\alpha = \frac{h_a}{2}(-\mathbf{v}_{2a}^t - \alpha\,\mathbf{v}_{3a}^t) \quad \text{and} \quad \mathbf{p}_a^\beta = \frac{h_a}{2}(\mathbf{v}_{1a}^t - \beta\,\mathbf{v}_{3a}^t) \tag{28}$$

Furthermore, the variation of Eqs. (20) yields:

$$\delta\boldsymbol{\beta} = \sum_{a=1}^{np} \begin{bmatrix} R_{a,x} & 0 & 0 & p_{a_x}^\alpha\,H_{a,x} & p_{a_x}^\beta\,H_{a,x} \\ R_{a,y} & 0 & 0 & p_{a_x}^\alpha\,H_{a,y} & p_{a_x}^\beta\,H_{a,y} \\ R_{a,z} & 0 & 0 & p_{a_x}^\alpha\,H_{a,z} & p_{a_x}^\beta\,H_{a,z} \\ 0 & R_{a,x} & 0 & p_{a_y}^\alpha\,H_{a,x} & p_{a_y}^\beta\,H_{a,x} \\ \vdots & \vdots & \vdots & \vdots & \vdots \\ 0 & 0 & R_{a,z} & p_{a_z}^\alpha\,H_{a,z} & p_{a_z}^\beta\,H_{a,z} \end{bmatrix} \begin{bmatrix} \delta u_a \\ \delta v_a \\ \delta w_a \\ \delta\alpha_a \\ \delta\beta_a \end{bmatrix} = \sum_{a=1}^{np} \mathbf{G}_a\,\delta\mathbf{u}_a = \mathbf{G}\,\delta\mathbf{u}, \tag{29}$$

Therefore, the virtual strains can be written as

$$\delta\boldsymbol{\varepsilon} = \overline{\mathbf{B}}\,\delta\mathbf{u}, \quad \overline{\mathbf{B}} = \mathbf{B}_0 + \mathbf{B}_L = \mathbf{H}\,\mathbf{G} + \mathbf{A}\,\mathbf{G} \tag{30}$$

Considering arbitrary virtual displacements ($\delta\mathbf{u}$) and displacement independent loads in Eq. (25) yields the nonlinear equilibrium equations:

$$\mathbf{r}(\mathbf{u}, \lambda) = \mathbf{g}(\mathbf{u}) - \lambda\,\mathbf{f}, \tag{31}$$

where:

$$\mathbf{g} = \int_V \overline{\mathbf{B}}^T\boldsymbol{\sigma}\,dV, \qquad \mathbf{f} = \int_V \mathbf{N}^T\,\mathbf{b}\,dV + \int_S \mathbf{N}^T\,\mathbf{q}\,dS, \tag{32}$$

and λ is the load factor. These equations should be solved in each step for $\mathbf{r} = 0$ using an appropriate path-following method, such as the Load Control, Displacements Control, or the Arc-Length Method, which are based on Newton-Raphson method iterations [8].

2.4 Tangent stiffness matrix

The stiffness matrix is obtained by the differentiation of the internal forces vector:

$$\mathbf{K}_T = \frac{\partial\mathbf{g}}{\partial\mathbf{u}} = \mathbf{K}_E + \mathbf{K}_G \tag{33}$$

From Eq. (32), the material stiffness matrix $\mathbf{K}_E$ and the geometric stiffness matrix $\mathbf{K}_G$ are given by:

$$\mathbf{K}_E = \int_V \overline{\mathbf{B}}^T\,\mathbf{C}\,\overline{\mathbf{B}}\,dV, \qquad \mathbf{K}_G = \mathbf{K}_{G_1} + \mathbf{K}_{G_2} + \mathbf{K}_{G_3}, \tag{34}$$

where $\mathbf{K}_{G_1}$ is the classical geometric stiffness matrix

$$\mathbf{K}_{G_1} = \int_V \mathbf{G}^T\,\mathbf{S}\,\mathbf{G}\,dV, \quad \mathbf{S} = \begin{bmatrix} \overline{\mathbf{S}} & \overline{\mathbf{0}} & \overline{\mathbf{0}} \\ \overline{\mathbf{0}} & \overline{\mathbf{S}} & \overline{\mathbf{0}} \\ \overline{\mathbf{0}} & \overline{\mathbf{0}} & \overline{\mathbf{S}} \end{bmatrix}, \quad \overline{\mathbf{0}} = \begin{bmatrix} 0 & 0 & 0 \\ 0 & 0 & 0 \\ 0 & 0 & 0 \end{bmatrix}, \quad \overline{\mathbf{S}} = \begin{bmatrix} \sigma_{xx} & \tau_{xy} & \tau_{xz} \\ \tau_{xy} & \sigma_{yy} & \tau_{yz} \\ \tau_{xz} & \tau_{yz} & \sigma_{zz} \end{bmatrix}. \tag{35}$$

The geometric stiffness matrices $\mathbf{K}_{G_2}$ and $\mathbf{K}_{G_3}$ appear due to the use of a nonlinear update scheme for the normal vector. These matrices are obtained using the methodology presented by Surana [10] considering Eqs. (14) and (28).

2.5 Integration and locking

Due to the use of the degenerated solid approach, a 3D integration scheme is adopted, where only two points are required in the thickness direction (ζ) due to the use of the Reissner-Mindlin theory. On the other hand, the full integration in the surface directions (ξ, η) requires $p+1$ integration points for each parametric coordinate, where p is the degree of the basis functions.

Unfortunately, the use of NURBS basis functions does not remove the shear and membrane locking presented by fully integrated shell elements based on Reissner-Mindlin kinematics, especially for thin-walled shells and low-order approximations [3]. Furthermore, the use of higher-order displacement approximations reduces but does not eliminate locking, so several techniques are used to alleviate the locking problem, such as uniform reduced integration and selective reduced integration [4].

It is well known that the uniform reduced integration scheme (R_{FEM}) using p integration points for each surface parametric coordinate alleviate, but not eliminate, locking of Reissner-Mindlin finite elements, while also generating spurious (or hourglass) modes.

On the other hand [4], presented a isogeometric reduced integration scheme (R_{IGA}) that eliminates shear and membrane locking in NURBS-based linear analysis of shells. Owing to the high regularity of NURBS basis functions with C^{p-1} continuity obtained through k-refinement, this approach simultaneously increases the accuracy and computational efficiency of IGA formulation, without generating spurious modes.

Therefore, the accuracy of Full, R_{FEM} and R_{IGA} integration schemes for geometrically nonlinear analysis of shells is investigated in considering well-known benchmarks [11].

3 Numerical Example

The accuracy of the proposed formulation considering different numerical integration schemes is assessed using a well-known benchmark, corresponding to the nonlinear analysis of a hemisphere with a pole cut of 18° and subjected to two pairs of loads located at antipodal points on the equator [11]. Due to the symmetry, only a quarter of the structure is modeled, as shown in Figure 1(a). This figure also presents the geometry, material properties, and boundary conditions. The shell is discretized using cubic NURBS meshes using Full, uniform reduced (R_{FEM}), and isogeometric reduced (R_{IGA}) integration schemes.

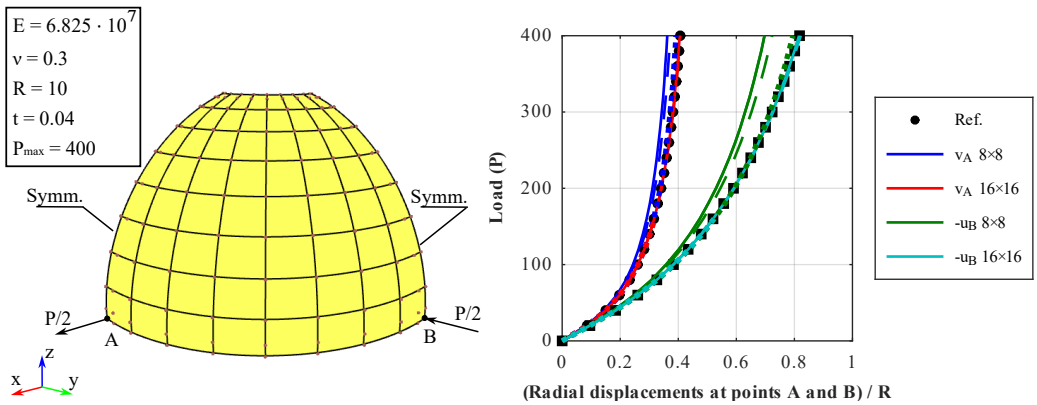

(a) Problem definition and 8×8 cubic mesh. (b) Full (solid), R_{FEM} (dashed), R_{IGA} (dotted) load-deflection curves.

Figure 1. Hemispherical shell under point loads.

The Load Control Method with Newton-Rapshon iterations was used to perform the nonlinear analyses. The load was applied using 20 uniform increments and the adopted tolerance for the force residual was 10^{-4}. Figure 1(b) shows the nonlinear load-deflection curves. The (R_{IGA}) integration scheme presents a better accuracy, especially for coarse discretizations. However, the results for the finer mesh (16×16) do not describe the complete curve, reaching only 0.4 of the load factor.

With the refinement of the model, all integration schemes converged to the expected solution, so that the results with the three integration schemes are almost identical to the reference. Finally, the results show that the reduced integrations alleviate the locking problem, leading to a faster convergence. Also, as the computational cost of uniform reduced integration is lower, this is a promising choice due to its efficiency.

Table 1 presents the number of iterations required to obtain the load-displacement curve for each integration scheme. Quadratic convergence was obtained for all cases, except for R_{IGA} with $16x16$ mesh. The convergence

behavior of Full and R_{FEM} is practically identical.

Table 1. Total (TotIter) and average (AvgIter) number of iterations for each mesh and integration scheme.

Mesh	8x8			16x16		
Integration	Full	R_{FEM}	R_{IGA}	Full	R_{FEM}	R_{IGA}
TotIter	112	113	122	119	120	261
AvgIter	5.60	5.65	6.10	5.95	6.00	32.62

4 Conclusion

This work presented a NURBS-based isogeometric formulation for geometrically nonlinear analysis of shells. The total Lagrangian formulation is employed allowing for large displacements and rotations. A simple and efficient scheme is adopted to update the director vector, removing the restriction of small nodal rotations between two successive load increments and providing quadratic convergence of equilibrium iterations.

Concerning the element integration, the results showed that isogeometric reduced integration can eliminate locking even in coarser meshes. However, it presented convergence problems for finer meshes. On the other hand, the uniform reduced integration scheme helps alleviate the locking phenomenon, improving result accuracy and computational efficiency. However, full integration schemes tend to converge to the same solutions with model refinement.

Further research will be carried out on the behavior of the proposed formulation for shells with other geometries and loads, focusing on structural stability problems.

Acknowledgements. The authors gratefully acknowledge the financial support provide by CNPq (Conselho Nacional de Desenvolvimento Científico e Tecnológico) and FUNCAP (Fundação Cearense de Apoio ao Desenvolvimento Científico e Tecnológico).

Authorship statement. The authors hereby confirm that they are the sole liable persons responsible for the authorship of this work, and that all material that has been herein included as part of the present paper is either the property (and authorship) of the authors, or has the permission of the owners to be included here.

References

[1] T.-K. Uhm and S.-K. Youn. T-spline finite element method for the analysis of shell structures. *International Journal for Numerical Methods in Engineering*, vol. 80, n. 4, pp. 507–536, 2009.

[2] W. Dornisch, S. Klinkel, and B. Simeon. Isogeometric reissner–mindlin shell analysis with exactly calculated director vectors. *Computer Methods in Applied Mechanics and Engineering*, vol. 253, pp. 491–504, 2013.

[3] R. Echter and M. Bischoff. Numerical efficiency, locking and unlocking of nurbs finite elements. *Computer Methods in Applied Mechanics and Engineering*, vol. 199, n. 5-8, pp. 374–382, 2010.

[4] C. Adam, S. Bouabdallah, M. Zarroug, and H. Maitournam. Improved numerical integration for locking treatment in isogeometric structural elements. part ii: Plates and shells. *Computer Methods in Applied Mechanics and Engineering*, vol. 284, pp. 106–137, 2015.

[5] G. Farin. *Curves and surfaces for computer-aided geometric design: a practical guide*. Elsevier, 2014.

[6] J. Argyris. An excursion into large rotations. *Computer methods in applied mechanics and engineering*, vol. 32, n. 1-3, pp. 85–155, 1982.

[7] K. J. Bathe. *Finite element procedures*. Klaus Jurgen Bathe, 2 edition, 2014.

[8] M. Crisfield. *Non-linear Finite Element Analysis of Solids and Structures: Essentials*. Non-linear Finite Element Analysis of Solids and Structures. Wiley, 1991.

[9] R. D. Cook and others. *Concepts and applications of finite element analysis*. John wiley & sons, 2007.

[10] K. S. Surana. Geometrically nonlinear formulation for the curved shell elements. *International Journal for Numerical Methods in Engineering*, vol. 19, n. 4, pp. 581–615, 1983.

[11] K. Sze, X. Liu, and S. Lo. Popular benchmark problems for geometric nonlinear analysis of shells. *Finite elements in analysis and design*, vol. 40, n. 11, pp. 1551–1569, 2004.